Full Length Article

Precision of bone mechanoregulation assessment in humans using longitudinal high-resolution peripheral quantitative computed tomography *in vivo*

Matthias Walle [a], Danielle E. Whittier [a,b], Denis Schenk [c], Penny R. Atkins [a,b], Michael Blauth [d], Philippe Zysset [c], Kurt Lippuner [b], Ralph Müller [a], Caitlyn J. Collins [a,e,*]

[a] *Institute for Biomechanics, ETH Zurich, Zurich, Switzerland*
[b] *Department of Osteoporosis, Bern University Hospital, University of Bern, Bern, Switzerland*
[c] *ARTORG Center for Biomedical Engineering Research, University of Bern, Bern, Switzerland*
[d] *Department of Orthopaedics and Traumatology, Medical University Innsbruck, Innsbruck, Austria*
[e] *Virginia Tech, Department of Biomedical Engineering and Mechanics, Blacksburg, VA, United States*

A B S T R A C T

Local mechanical stimuli in the bone microenvironment are essential for the homeostasis and adaptation of the skeleton, with evidence suggesting that disruption of the mechanically-driven bone remodelling process may lead to bone loss. Longitudinal clinical studies have shown the combined use of high-resolution peripheral quantitative computed tomography (HR-pQCT) and micro-finite element analysis can be used to measure load-driven bone remodelling *in vivo*; however, quantitative markers of bone mechanoregulation and the precision of these analyses methods have not been validated in human subjects. Therefore, this study utilised participants from two cohorts. A *same-day cohort* (n = 33) was used to develop a filtering strategy to minimise false detections of bone remodelling sites caused by noise and motion artefacts present in HR-pQCT scans. A *longitudinal cohort* (n = 19) was used to develop bone imaging markers of trabecular bone mechanoregulation and characterise the precision for detecting longitudinal changes in subjects. Specifically, we described local load-driven formation and resorption sites independently using patient-specific odds ratios (OR) and 99 % confidence intervals. Conditional probability curves were computed to link the mechanical environment to the remodelling events detected on the bone surface. To quantify overall mechanoregulation, we calculated a correct classification rate measuring the fraction of remodelling events correctly identified by the mechanical signal. Precision was calculated as root-mean-squared averages of the coefficient of variation (RMS-SD) of repeated measurements using scan-rescan pairs at baseline combined with a one-year follow-up scan. We found no significant mean difference ($p < 0.01$) between scan-rescan conditional probabilities. RMS-SD was 10.5 % for resorption odds, 6.3 % for formation odds, and 1.3 % for correct classification rates. Bone was most likely to be formed in high-strain and resorbed in low-strain regions for all participants, indicating a consistent, regulated response to mechanical stimuli. For each percent increase in strain, the likelihood of bone resorption decreased by 2.0 ± 0.2 %, and the likelihood of bone formation increased by 1.9 ± 0.2 %, totalling 38.3 ± 1.1 % of strain-driven remodelling events across the entire trabecular compartment. This work provides novel robust bone mechanoregulation markers and their precision for designing future clinical studies.

1. Introduction

The bone remodelling process is a complex mechanism that enables structural adaptation to align with physiological loading conditions, such as gravitational loading or muscle forces, thereby minimising the risk of bone fractures [1]. At the cellular level, this process is orchestrated by osteocytes, which sense local mechanical forces and signal bone-forming cells in regions where mechanical stimulations are high, and bone-resorbing cells in areas where the stimulus is low [2–4]. This mechanoregulated exchange of old bone for newly formed material

---

reduces fatigue damage and promotes skeletal strength [5]. However, the ageing skeleton is believed to respond less effectively to mechanical stimuli, such as loading induced by physical exercise [6–8]. The discordant mechanoregulation of bone due to ageing and disease may be attributed to decreased osteoblast activity and increased apoptosis [9,10], increased osteoclast number [11], or declining osteocyte density [12,13]. This loss of mechanoregulative response may also occur from various chronic diseases, including diabetes mellitus [14]. Previous biological observations may explain the loss of bone volume, quality, and strength *ex vivo*, but they do not give conclusive proof of potentially dysregulated mechanoregulation in living bone tissue. Therefore, approaches for monitoring *in vivo* bone microstructure at high resolution are necessary to explore the effects of ageing and diseases on bone remodelling in humans.

High-resolution peripheral quantitative computed tomography (HR-pQCT) can non-invasively assess individual trabecular structures *in vivo* in humans with nominal resolution ranging from 61 μm to 82 μm achieving spatial resolutions between 95.2 μm and 142.2 μm *in vivo* [15,16]. Acquisition of longitudinal images can even allow for the quantification and visualisation of remodelling sites [17]. When HR-pQCT is combined with micro-finite element (micro-FE) analysis, the local mechanical environment can be simulated and linked to remodelling events (*i.e.* mechanoregulation). Previous clinical studies exploring mechanoregulation in humans [18–21] have demonstrated relationships between local strains induced by normal physiological activity and bone remodelling, showing promise for HR-pQCT-based mechanoregulation to investigate the effects of disease, ageing, or intervention on the skeleton's ability to adapt to mechanical stimuli. However, the resolution of HR-pQCT is in the same order of magnitude as the depth of individual remodelling sites (between 5 and 116 μm) [22,23]. To overcome the current limitation of imaging resolution, image filtering protocols are necessary to remove noise and image artefacts that can overshadow these subtle changes [17].

The studies by Christen et al. and Mancuso et al. have estimated the precision of analysing bone remodelling sites derived from same-day repeat scans and reported a broad range of measurement precision ranging from 2.5 % [17] to 11 % [18]. Image noise and motion artefacts during scanning can confound the precision of longitudinal bone microstructure assessment [17]. To reduce false detections, previous studies have proposed noise-filtering protocols [17]. However, with the recent advancements from a nominal resolution of 82 μm to 61 μm in second-generation XtremeCT scanners, previous filtering methods must be revised to account for differences in image resolution, artefacts, and noise. Importantly, these assessments only considered the overall rate of false detections without considering the variations in the spatial location of the bone remodelling sites. Previous imaging-based assessments of bone mechanoregulation [19,24,52] correlate the mechanical signal with local remodelling events voxel-by-voxel. Therefore, the spatial variance of these remodelling sites may have a significant impact on the quantification of remodelling sites relative to local mechanical strains and needs to be assessed using longer follow-up scans during which true remodelling events take place. A major challenge with assessing bone formation/resorption using HR-pQCT is the limited availability of validation data (e.g., dynamic histomorphometry) for humans [53]. Assessing the precision in estimating mechanoregulation of local bone remodelling is critical for determining whether measured differences within or across patients are due to genuine changes or caused by noise and artefacts.

This study aimed to develop bone mechanoregulation imaging markers and to determine their precision for detecting longitudinal changes in human subjects. In this context, precision describes the consistency of measurements obtained by a single team using the same procedure, equipment, and operating conditions, in a single location, over multiple iterations [25]. The first objective of this study was to adapt an existing image filtering protocol for detecting local bone formation and resorption sites to current imaging capabilities, and to evaluate the effect of motion artefacts on the accuracy and precision of the adapted filtering approach. The second objective of this study was to establish robust patient-specific markers that characterise strain-driven bone formation and bone resorption as well as their interplay (*i.e.*, mechanoregulation).

2. Methods

2.1. Participants and image acquisition

This study utilised participants from two cohorts, summarised in the following paragraphs, to address each study objective. The first is the *same-day cohort*, used to assess filtering parameters designed to remove false formation and resorption sites. The second cohort is referred to as the *longitudinal cohort*, used to determine the precision of mechanoregulation over one year of bone remodelling. All participants gave written informed consent before participation, and local ethics committees approved all studies. All scans were obtained at the distal radius using second-generation HR-pQCT (XtremeCT II, Scanco Medical AG, 61 μm) [15]. For consistency across cohorts, scans were automatically graded for motion artefacts using a previously developed motion-scoring algorithm [26] on a five-point scale (1 = none, 2 = minor, 3 = moderate, 4 = severe, and 5 = extreme), with manual verification.

The *same-day cohort* consisted of 33 participants (17 males of mean age 46.2 ± 18.4 years; 16 females of mean age 41.3 ± 15.8 years) from a previous study [27]. Three same-day HR-pQCT scans of the distal radius were acquired at the University Department of Osteoporosis in Bern for all participants. Individuals were scanned by the same operator with two operators in total. After each scan, the carbon cast was removed, reapplied, and the subject was repositioned. The scan region used herein began at the reference line placed at the dense articular surface formed with the scaphoid and lunate fossae of the radiocarpal joint and extended proximally 10.2 mm (168 slices) in length [28].

The *longitudinal cohort* consisted of 19 participants (9 males of mean age 43.9 ± 13.1 years; 10 females of mean age 59.1 ± 18.9 years) selected from an ongoing multi-centre longitudinal study investigating fracture healing [29], where longitudinal scans acquired on the contralateral (*i.e.* non-fractured distal radius) were used in the present study. Three scans were used per participant, including a baseline scan, a 1-month repeat scan performed within one month, and a third scan performed at a one-year follow-up. Scans were obtained from a previous study at the Innsbruck Medical University in Innsbruck, Austria [30], or newly acquired at the University Department of Osteoporosis in Bern, Switzerland. Participants were included from the more extensive longitudinal study if they had attended all three visits and all scans had a motion score of 2 or lower (on the five-point scale), resulting in 19/132 participants that met the inclusion criteria. In this cohort, HR-pQCT scans were acquired following the manufacturer's standard *in vivo* protocol [31]. Briefly, a reference line was placed on the distal radial joint surface using anteroposterior scout views. The scan region (168 slices) was 10.2 mm extended, positioned at a fixed offset of 9.0 mm from the reference line.

2.2. Image processing and registration

Periosteal and endocortical contours were automatically identified in all images using the dual-threshold technique (cortical bone: 450 mg HA/cm^3, trabecular bone: 320 mg HA/cm^3) [32]. Contours were visually inspected for notable deviations from the periosteal or endocortical surfaces and manually corrected where necessary [33]. HR-pQCT scans were registered using rigid-body registration based on Python (v3.8.5) and SimpleITK (v2.1.1.2) [34,35]. Specifically, Euler angles around the density-weighted centre of the image were optimised, maximising the voxel-wise correlation between grayscale density values within the periosteal contour to align the images. Powell optimisation with Brent line search, an initial step length of 1, and a sampling rate of 0.01 in

conjunction with a five-level pyramid registration framework (shrink factors: $12\times, 8\times, 4\times, 2\times, 1\times$) was used. Optimisations terminated after 100 iterations or if the value or step tolerance of 10^{-6} was reached. Grayscale images were transformed using linear interpolation, and a Gaussian filter was applied to reduce noise (sigma 1.2, support 1). Binary segmentations of the bone and compartment masks (cortical and trabecular) were transformed using nearest-neighbour interpolation. In all cases, the earliest timepoint was used as the fixed reference image, and all follow-up images were transformed into the reference space.

2.3. Objective 1: bone remodelling site identification and quantification of precision

Image filtering parameters needed to identify true bone formation and resorption fractions were determined using the *same-day cohort*. Due to the short follow-up time (same-day scans), no measurable true bone remodelling is expected, and thus all detected remodelling events can be considered false remodelling sites. First, the common trabecular region across rescans was determined from the registered images to exclude voxels outside the common region. Segmented images were then superimposed to identify regions of false formation and resorption in the trabecular compartment. Volumes of the segmented bone present only in the earlier measurement were regarded as resorbed bone, whereas bone voxels present only in the latter measurement corresponded to formed bone [24]. For the same-day scans, all possible combinations of the three measurements were evaluated. To reduce the detection of false remodelling events caused by registration interpolation and partial-volume effects, the identified formation and resorption sites were further filtered using information from the grey-scale images to remove small remodelling clusters or sites with minimal density changes [17]. For this purpose, the threshold for the absolute difference in density between rescans of the formed and resorbed voxels was varied from 0 to 300 mg HA/cm^3 with a step size of 25 mg HA/cm^3, and the threshold for cluster volume was varied from 0 to 48 voxels in steps of 4 voxels. The proportion of removed remodelling clusters was calculated at different filter combinations, and filtering settings within a tolerable 1 % noise level were selected to remove false remodelling sites. Finally, formation and resorption volumes were expressed as a fraction of the baseline trabecular mineralised bone volume (Tb.BV).

Short-term precision of formation and resorption measurements were calculated as root-mean-squared averages of the standard deviation of repeated measurements (RMS-SD) [36] Individual precision errors were calculated for resorption (Tb.R) and formation (Tb.F) volume fractions derived from combinations of scan/rescan pairs. For example, for a patient with three scans (t_{1-3}), the following comparisons (c_{1-3}) between detected resorption fractions were made with c_1: RMS-SD(Tb.$R_{t2,t3}$, Tb.$R_{t1,t3}$), c_2: RMS-SD(Tb.$R_{t2,t3}$, Tb.$R_{t1,t2}$), and c_3: RMS-SD(Tb.$R_{t1,t2}$, Tb.$R_{t1,t3}$) and grouped by the maximum motion score of all scans within the comparison. Differences in precision outcomes between grading scores were tested with an unpaired Mann-Whitney-Wilcoxon test with Holm–Bonferroni correction for multiple comparisons after confirming the non-normality of variables with a Shapiro-Wilk test. Least-significant change of bone Tb.F and Tb.R was calculated at a 95 % confidence level (where LSC = 2.77 * RMS-SD) [36] with the developed filtering approach and compared against no filtering steps applied (*i.e.* remodelling sites obtained from subtracted segmented images).

2.4. Objective 2: bone mechanoregulation quantification over one year

The precision of detecting remodelling sites and bone mechanoregulation was evaluated in a longitudinal cohort using three scans: baseline, 1-month repeat, and 1-year follow-up (Fig. 1A). The evaluation was conducted between the baseline and 1-year scans, as well as between the 1-month and 1-year scans, as it requires the presence of true bone formation and resorption sites. The formation and resorption sites occurring after a one one-year interval were identified using the optimised filtering approach determined in objective 1. A paired Wilcoxon signed-rank test was used to determine the presence of substantial bone resorption, formation, and net change between baseline and one year, after confirming the non-normality of variables with a Shapiro-Wilk test. The approach was performed again with the repeat scan (taken within one month of the baseline) in place of the baseline scan to test the agreeability of the approach (Fig. 1B). Bland-Altman plots were used to measure the limits of agreement between baseline and 1-month repeat scans when determining the resorption, formation, and net change fraction after one year.

The local mechanical signal in the bone tissue of the baseline scan was calculated using micro-FE analysis (Fig. 1C). Finite element meshes were generated by converting all voxels to 8-node hexahedral elements and assigning a Young's modulus of 8.748 GPa and Poisson's ratio of 0.3
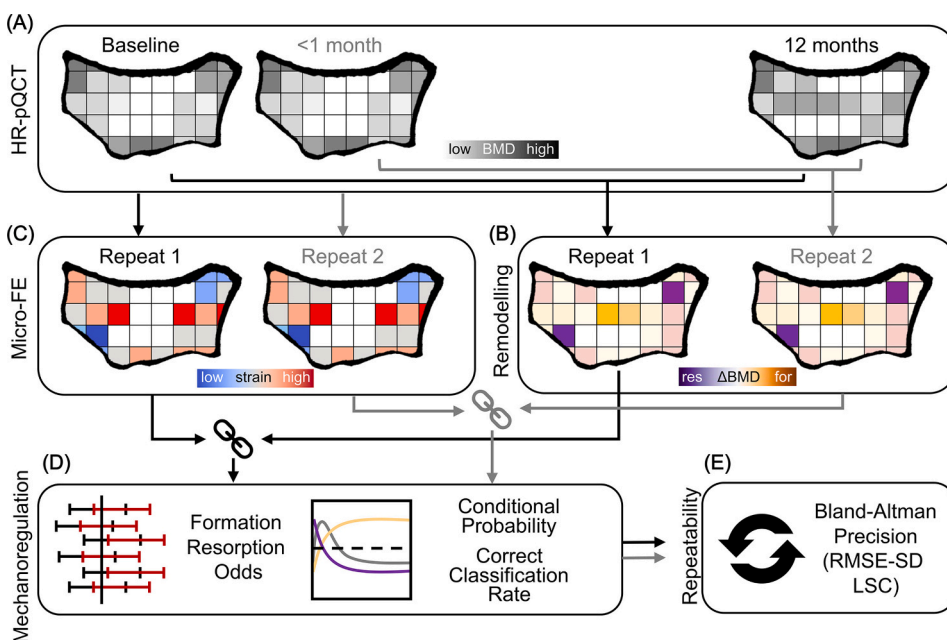

Fig. 1. Study design for objective 2. (A) Baseline and repeat scans were acquired within one month, along with a one-year follow-up for each patient (n = 19) using HR-pQCT to measure bone mineral density (BMD) and microstructure. (B) Remodelling sites were identified from segmented images and filtered in the greyscale image based on changes in density between baseline and follow-up as well as 1-month repeat and follow-up. (C) Micro-FE analysis was performed on the baseline and 1-month repeat scans. (D) Mechanoregulation was assessed using quantitative markers. (E) The precision of mechanoregulation markers was assessed.

[37]. A standard uniaxial compression of up to 1 % apparent strain was applied. Linear micro-FE calculations were solved using ParOsol [38] at the ETH research computing cluster (Euler, ETH Zurich, Zurich, Switzerland) using 48 threads (Intel Xeon Gold 5118, 3.2 GHz, 96 GB). Voxel-wise strain energy density (SED) was derived as the local mechanical signal [19,24].

Following the method presented by Schulte et al. [24], patient-wise conditional probability curves were computed to link the mechanical signal (baseline SED) at different strain levels to the remodelling events detected on the bone surface between baseline and the one-year follow-up (Fig. 1D). Briefly, SED was normalised using the 99th percentile and binned at 1 % intervals ($n_{bins} = 100$). Conditional probability was calculated from strain frequency distributions to analyse the probability of bone remodelling events at various strain levels. The conditional probability curves were used to calculate the correct classification rate (CCR), a measure for estimating the proportion of remodelling events (resorption, quiescence, and formation) correctly relative to mechanical signal [39]. However, CCR only provides an overall marker of agreeability, not an independent assessment of the extent to which formation and resorption events are load-driven. Thus, logistic regression was performed to independently ascertain the patient-specific association between mechanical signal (baseline SED) with voxel-wise bone formation and resorption. Odds ratios for bone resorption (OR_R) formation (OR_F) with 99 % confidence intervals (CI) were computed per one-percentage-point change in normalised mechanical signal (SED/SED_{max}) to quantify strain-driven bone formation and resorption in individual participants. The 99 % CIs were constructed using bootstrapping (k = 1000). A confidence interval of 99 % was used due to the large sample size when performing voxel-wise analysis.

The mechanoregulation analysis was repeated using the repeat scan (taken within one month of the baseline) in place of the baseline scan to determine the precision of the approach. [45]. Bland-Altman plots, with 99 % CI were used to measure the limits of agreement between baseline and 1-month repeat scans in estimating the conditional probability of resorption, quiescence and formation events for each strain bin ($n_{bins} = 100$). One-year RMS-SD and least-significant change of OR_R, OR_F, and CCR were calculated using outcomes of the baseline-to-one-year and repeat-to-one-year pairs to assess the method's precision.

3. Results

3.1. Objective 1: bone remodelling sites identification and precision

After identifying the location of remodelling sites from segmented images, then removing detected remodelling events with a density change lower than 225 mg HA/cm³ and clusters smaller than 12 voxels, 99% of false remodelling sites observed in the same-day cohort were eliminated (Fig. 2A). The remaining 1 % of false remodelling sites were considered acceptable noise levels (supplemental Figure S1). Overall, filtering significantly improved ($p < 0.01$) absolute errors in the detection of false formation and resorption sites across all motion scores (Fig. 2B and Table 1). When assessing the absolute errors relative to motion scores after filtering, no significant differences were found for scans with motion scores of one or two. However, when at least one scan in the scan-rescan pair had a motion score of three or more, absolute errors significantly increased ($p < 0.01$), despite implementing the optimised filtering protocol. Specifically, when the maximal motion score in scan-rescan pairs shifted from two to three, the detection of false resorption events increased from 6.0 % to 11.3 % and false formation events increased from 6.4 % to 11.9 %. Therefore, scans with motion scores one or two were selected for further processing in the longitudinal cohort.
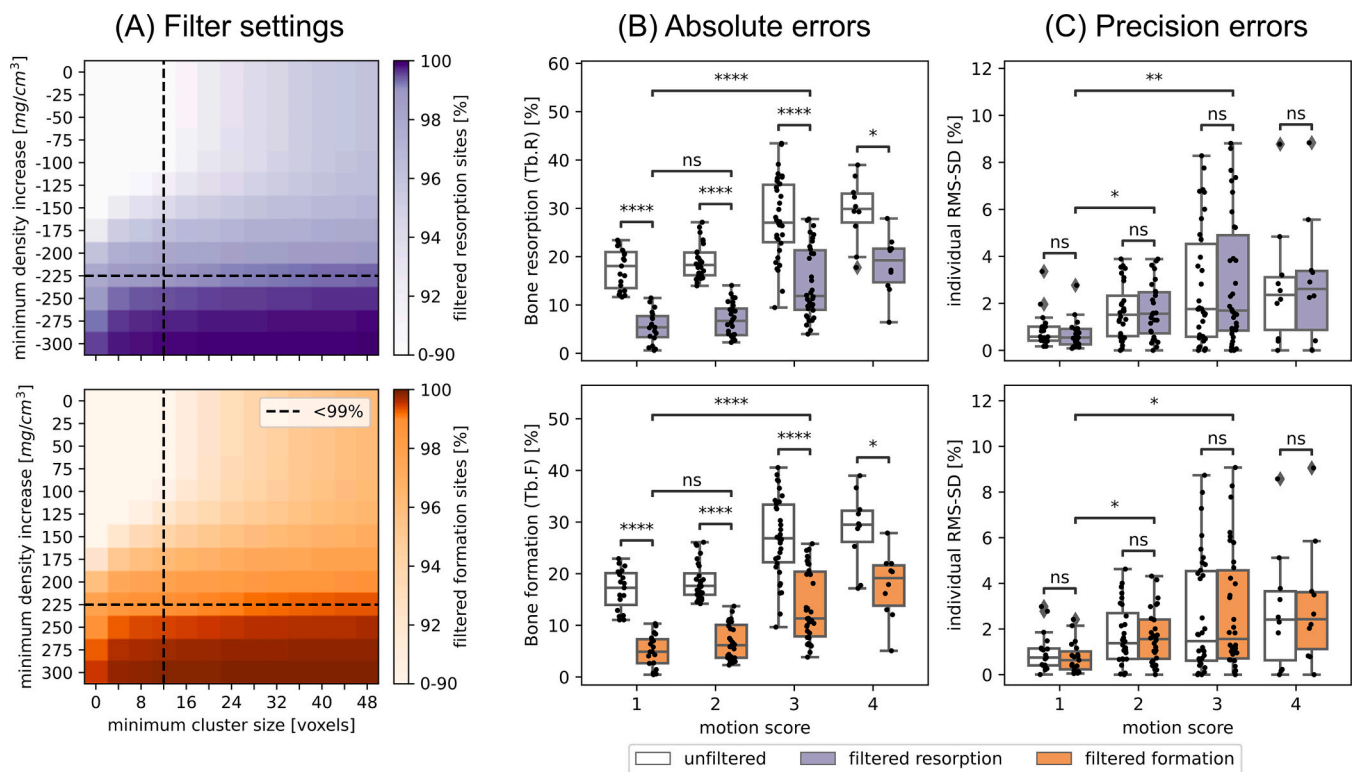

Fig. 2. (A) Filter strategy determined using three same-day rescans of participants (n = 33). The colour code indicates the percentage of filtered formation and resorption sites identified from binary segmentations and subsequent density change thresholds using different filter combinations. (B) Absolute errors were calculated assuming no true bone remodelling between scans. Boxplots show absolute errors with and without filtering for formation and resorption fractions at different motion scores. (C) Precision errors expressed as RMS-SD between individual measurements were grouped by maximum motion score within the comparison set. Boxplots show precision errors with and without filtering for formation and resorption fractions at different motion scores. Significant differences are indicated ($*p < 0.05$; $**p < 0.01$, $****p < 0.0001$, Mann-Whitney-Wilcoxon test with Holm–Bonferroni correction).

Table 1

Precision errors for resorption (Tb.R) and formation (Tb.F) detections expressed as standard deviation of repeated measurements (RMS-SD) and least-significant change (LSC). Measurements were grouped progressively restricting inclusion criteria for patient motion. Maximum motion score indicates the highest motion score tolerated.

Maximum motion score	Degrees of freedom	Abs. error (95 % CI)		RMS-SD		LSC	
		Tb.F	Tb.R	Tb.F	Tb.R	Tb.F	Tb.R
≤4	58	9.2 % (6.9 %–11.5 %)	9.8 % (7.2 %–12.3 %)	3.2 %	3.3 %	9.0 %	9.2 %
≤3	50	9.2 % (6.6 %–11.8 %)	9.7 % (6.9 %–12.6 %)	2.9 %	3.0 %	7.9 %	8.2 %
≤2	26	6.1 % (4.2 %–8.0 %)	6.4 % (4.5 %–8.2 %)	1.7 %	1.7 %	4.6 %	4.7 %
=1	10	4.5 % (1.1 %–7.9 %)	4.8 % (1.6 %–8.1 %)	0.9 %	0.7 %	2.4 %	1.8 %

The precision error of formation and resorption events was unchanged ($p = 1.0$) by the added filtering protocol across all motion scores. However, the precision of bone formation and resorption events significantly improved with lower motion grading ($p < 0.05$, Fig. 2C and Table 1). Overall, the precision of detecting bone formation *versus* resorption events was comparable across image quality gradings (RMS-SD = 3.3 %, for all scans, and RMS-SD = 1.7 % for motion scores of two or less). Overall, these results confirm that motion artefacts play a considerable role in the method's precision, while image filtering significantly influences absolute errors of false remodelling events.

3.2. Objective 2: precision of bone mechanoregulation analysis

In the longitudinal cohort, removing remodelling events with a density change lower than 225 mg HA/cm^3 and clusters smaller than 12 voxels (as determined in objective 1) visually reduced the amount of detected formation and resorption sites relative to the unfiltered approach, and the filtering strategy showed good precision between baseline repeat measurements (Fig. 3). We found significant bone resorption of 5.3 % (95 % CI: 3.1 %–7.5 %, $p < 0.05$) and formation of 5.2 % (95 % CI: 3.0 %–7.4 %, $p < 0.05$) after one year compared to resorption of 3.7 % (95 % CI: 2.4 %–5 %, $p < 0.05$) and formation of 3.1 % (95 % CI: 1.7 %–4.5 %, $p < 0.05$) within one month, between baseline and the 1-month repeat scan (Fig. 4A). Bland-Altman plots showed no significant bias ($p < 0.01$) between baseline and repeated scans for deriving one-year bone formation and resorption volume fractions. The 95 % limits of agreement identified one participant with high bone resorption (Tb.R > 6.6 %) and formation (Tb.F > 6.7 %) as an outlier (Fig. 4B).

In terms of mechanoregulation outcomes over the one-year follow-up, we found that bone had the highest conditional probability to be formed in high-strain and resorbed in low-strain regions (Fig. 5A), and no bias ($p < 0.01$) was found between conditional probabilities computed when using the baseline *versus* 1-month repeat scan (Fig. 5B). No participants showed a dysregulated response (OR < 1.0 or CCR < $^1/_3$) to mechanical stimuli. The range of participant-level OR_R was between 1.3 and 3.5, and OR_F was between 1.3 and 2.9 (Fig. 5C). The overall population showed that the likelihood of bone resorption was

significantly associated with decreasing strain, and bone formation was significantly associated with increasing strain, with an overall OR_R of 2.0 (99 % CI: 1.8–2.2) and OR_F of 1.9 (99 % CI: 1.7–2.1). On average, 38.3 % (99 % CI: 37.2–39.4) of strain-driven remodelling events were detected with CCR, ranging from 35.7 % to 42.5 %. In most cases, confidence intervals between one-year mechanoregulation markers estimated from baseline and 1-month repeat scans showed consistent participant-level overlap, demonstrating good precision at the participant level. Visually, trending differences in OR_R, OR_F, and CCR between age and sex groups of participants were observed, yet no explicit comparisons were made due to insufficient statistical power. Precision errors of OR_R (RMS-SD = 0.2, RMS-CV = 10.5%, LSC = 0.6) were higher than OR_F (RMS-SD = 0.1, RMS-CV = 6.3%, LSC = 0.3). CCR showed excellent precision (RMS-SD = $5.1 * 10^{-3}$, RMS-CV = 1.3%, LSC = $14.0 * 10^{-3}$). Overall, bone mechanoregulation markers acquired from the baseline and 1-month repeat scans show consistent results on a participant-specific level, demonstrating the method's precision.

4. Discussion

Mechanical signals are one of the most important determinants of bone health in humans [40], yet, quantifying the metabolic response of bone tissue to this stimulation has proven difficult. Here, we demonstrated that longitudinal HR-pQCT at 61 μm nominal resolution can detect local bone formation and resorption on the bone surface over the course of one year. Combined with micro-FE analysis, we found a substantial temporospatial relationship between bone remodelling and local mechanical signals. We quantified the capacity of regional mechanical stimulus variations to initiate bone remodelling events using participant-specific formation and resorption odds ratios. We showed that local strain variations affected remodelling differently across participants. Further, we demonstrated that the proportion of remodelling events that were correctly correlated to the mechanical signal varied across participants. Using repeat scans, we evaluated the precision of this method to ensure that bone formation and resorption detected among individuals were not solely related to noise and measurement errors. Finally, our study provided robust *in vivo* mechanoregulation markers characterising the effect of local mechanical stimuli on bone remodelling and quantified their precision.

For a reliable evaluation of bone mechanoregulation, consistent detection of local bone formation and resorption sites is required. Using an independent same-day-repeat HR-pQCT cohort, we showed that filtering of remodelling sites based on density change and cluster volume can reduce false detections without adversely impacting the method's precision. The basis of the proposed filtering approach was first developed for the first generation of HR-pQCT (XtremeCT, ScancoMedical, 82 μm) [17]. Although the nominal resolution has increased from 82 μm to 61 μm, we found consistent filtering parameters of 225 mg/cm^3 minimum density change and 12 voxels minimum cluster size, which is equivalent to 5 voxels at 82 μm resolution, were effective for removing the majority (99 %) of false remodelling events. In contrast to the prior method the additional binary segmentation step used in this study likely removed already a majority of soft-tissue noise. Previous studies have shown that it is possible to retrospectively estimate specific second-generation HR-pQCT measurements from first-generation acquired images using cross-calibration techniques [41]. Our findings suggest that this could also be viable for mechanoregulation measurements, allowing comparisons to published longitudinal data at 82 μm resolution; however, future cross-calibration studies would be required to confirm this. Further, the LSC required to detect bone formation was comparable to the LSC required to detect resorption and did not change from the previous scanner generation [17]. We found that LSC rapidly increased with increasing patient motion, roughly 2 % for high-quality (score 1) and 5 % for good-quality (score 2) scans. Although the average volume replacement (turnover) of bone is approximately 10 % per year [42], it varies across different sites. It is estimated to be substantially lower at
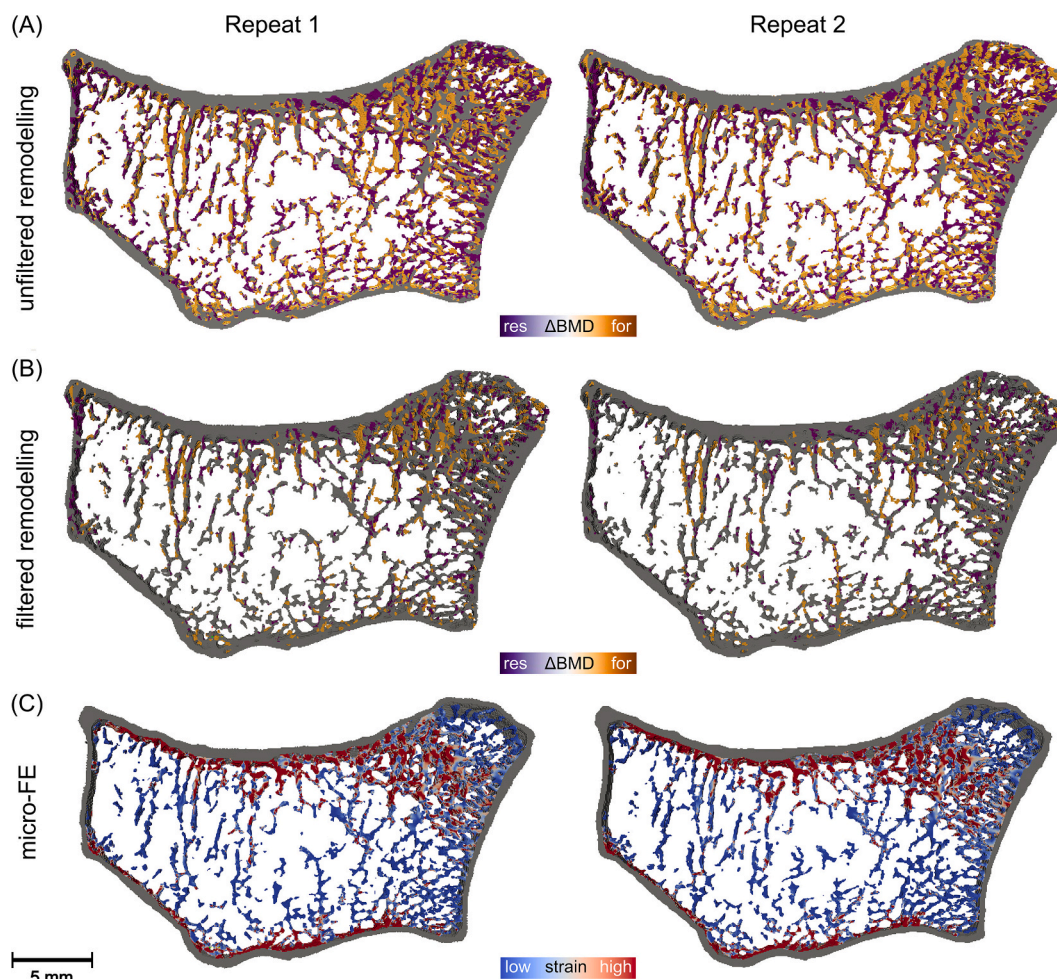
Fig. 3. (A) Representative axial cross-sections (15 slices thick) of the human distal radius show bone remodelling over one year. Sites of bone formation (for) and resorption (res) were determined using three-dimensional image registration of baseline and 1-year follow-up measurements for scans (repeat 1) and rescans (repeat 2). (B) Remaining formation and resorption sites are shown after filtering small remodelling clusters (<12 voxels) with a minimum change in density of ± 225 HA mg/cm^3, using the optimised filtering strategy from objective 1. (C) Corresponding micro finite element analysis (micro-FE) visually shows higher strain energy density in regions of formation and lower strain energy density in regions of resorbed bone.

yellow bone marrow sites, such as the distal radius, at roughly 2 % per year [43,44]. Our findings suggest that the proposed technique is a dependable *in vivo* method for measuring local bone turnover, as we observed similar increases in remodelling fractions over a year in our longitudinal cohort compared to previous estimates based on treatment response [43,44]. Although filtering can reduce false detections of formation and resorption events, our findings suggest future studies should only use low-motion HR-pQCT scans (motion $\leq$ 2), especially for short follow-ups or when investigating diseases with low bone turnover, such as diabetes mellitus. Differences observed in the current study compared to a previous study [17], recommending the inclusion of motion scores up to grade 3, may be due to operator variability of the manual motion scoring procedure [33]. To ensure inter-study comparability, we used a previously developed automatic motion grading system [26] to eliminate the subjectivity of motion scores. Studies may be able to use scans with moderate motion artefacts grade (motion grades 3) for more extended follow-up periods or when investigating bone diseases with more rapid changes, such as chronic kidney disease [45].

Our results indicate a consistent relationship between increasing strain and bone remodelling events, reflected in the odds of bone formation increasing by 1.9% and odds of bone resorption decreasing by 2.0% per percent increase in SED. The proposed quantification of bone mechanoregulation using correct classification rates (a trinary classification system) and odds ratios for bone formation and resorption

provides complementary information about the mechanoregulatory relationship between mechanical strains and bone remodelling events. While odds ratios measure the strength and direction of the association between local strains and bone remodelling, the correct classification rate measures the overall performance of strains in predicting the correct remodelling event. Our findings suggest that the consistent relationship observed in remodelling at the radius in an adult population is not entirely driven by mechanical factors, as evidenced by an average correct classification rate of 38.3%. These findings align with previous studies that have determined correct classification rates for both humans [20,21] and mice [39,56–58]. Non-mechanical bone remodelling could be influenced by a range of factors, such as calcium homeostasis, hormonal regulation, and inflammatory processes. Further, ageing and disease can have additional negative effects on bone remodelling that is both mechanically and biologically driven, which may confound interpretation of the mechanoregulation metrics we have proposed. Therefore, it is recommended that mechanoregulation analysis is assessed alongside bone formation and resorption volume fractions. This will enable a more comprehensive understanding of the impact of ageing on bone remodelling.

Understanding the mechanisms behind localised bone loss and turnover dynamics in response to strain patterns may have important implications for treating age-related or disease-induced bone loss [1]. For example, previous HR-pQCT studies have identified impaired bone
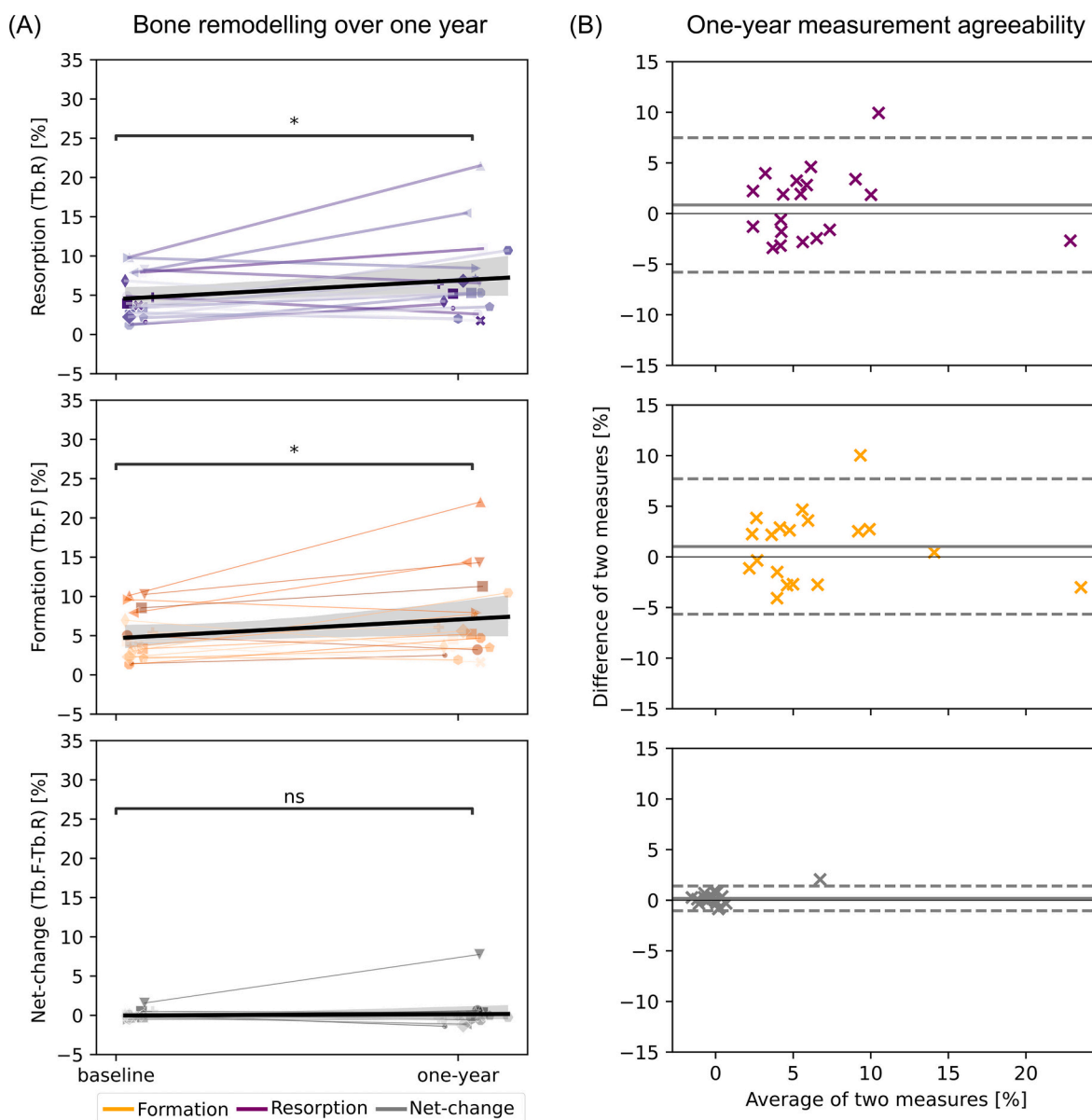
Fig. 4. (A) Bone resorption, formation and net change fraction with 95% confidence intervals (shaded area) over one year of bone remodelling assessed by longitudinal HR-pQCT imaging. Significant increases in remodelled tissue fraction from baseline to one year are indicated (*$p < 0.05$; Wilcoxon signed-rank test). (B) Bland-Altman plots illustrating the mean offset (solid mid-line, grey) and 95 % confidence limits (dashed lines, grey) of agreement for one-year resorption, formation, and net-change fractions when the baseline *versus* repeat scans (within one month of baseline) were used.

microstructure in patients with diabetes mellitus [46]. In these patients, observed microstructural deficits [47] may be directly related to an impaired response to mechanical loading, as has been observed in diabetic animal models [48]. Our proposed mechanoregulation method has the potential to bridge the gap between clinically observed bone phenotype and animal models and may help to develop mechanical intervention therapies that enhance bone health and lower fracture risk in diabetic patients. Through determination of the level of strain that constitutes bone growth and the level of strain that may be excessive and raise the risk of damage or failure, similar analysis methods could also be incorporated into personalised physiotherapy or exercise treatments. Further, interventions that improve mechanosensitivity, as measured using the techniques described herein, may provide novel treatments for these patients. In support of this, a previous study showed that bone mechanoregulation could be used to assess the effects of vitamin D and calcium supplementation in individuals [21]. Our findings provide the necessary precision for these and future studies to interpret observed

changes in mechanoregulation within and across participant groups.

A primary limitation of our study is that we focused exclusively on trabecular bone due to its high metabolic activity and anticipated frequent remodelling during the 1-year follow-up period. While investigating cortical bone remodelling and mechanoregulation may be possible, the surface-based mechanoregulation method used in this study was specifically designed for trabecular bone [24]. Cortical bone remodelling involves both surface and internal haversian remodelling, which may not be fully resolved using the resolution of HR-pQCT over a 1-year interval. Given these considerations, we did not extend the remodelling and mechanoregulation analysis to include cortical bone. Future research may introduce techniques to explore mechanoregulation in cortical bone, such as the recently suggested methods for investigating contractions and expansions of cortical pores [54]. Further, the employed micro-FE model was linear in terms of material and geometry. These simplifications do not account for nonlinear behaviour or viscoelastic effects; however, only minor linear-elastic
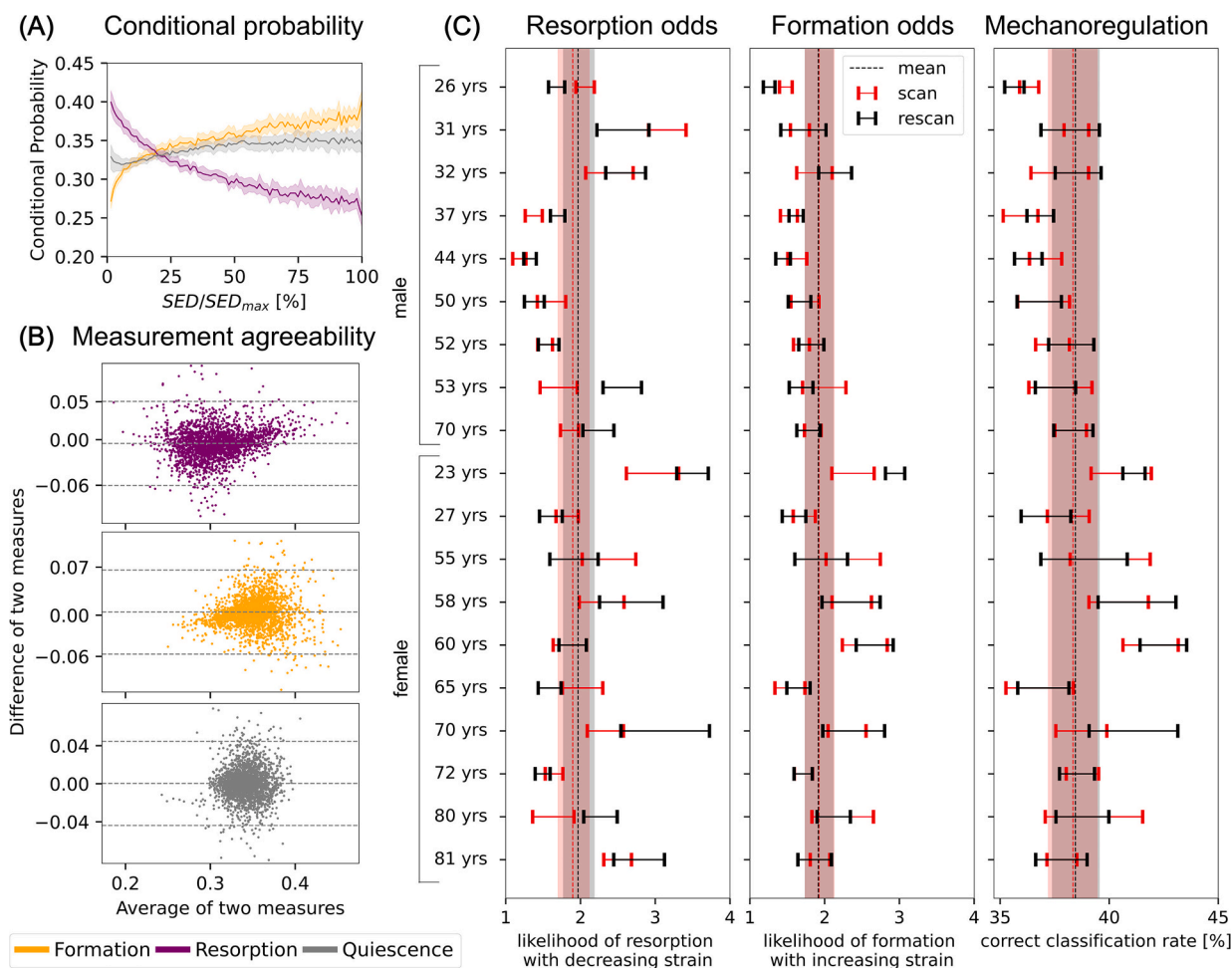
Fig. 5. (A) Conditional probability of bone resorption, quiescence, and formation throughout one year of bone remodelling (n = 19) with varying local strain energy density (SED) magnitudes. (B) Bland-Altman plots illustrate mean offset (solid mid-line, grey) and 95 % confidence limits (dashed lines, grey) of conditional probability agreement of a repeat assessment (<1 month) conducted on the same participant. (C) Respective odds ratios of bone resorption/formation with decreasing/increasing SED and correct classification rates quantify the mechanically-driven bone remodelling in participants. Vertical dashed lines indicate average measurement values, and the shaded area shows the 99 % confidence intervals for baseline scans (red) and 1-month repeat scans (black). (For interpretation of the references to colour in this figure legend, the reader is referred to the web version of this article.)

deformations are anticipated during daily activities [50]. Further the use of only compressive loading may not accurately reflect day-to-day loading patterns. However, our prior study demonstrated only modestly higher correct classification rates when utilising computational load estimation algorithms that aims to more accurately estimate true day-to-day loading conditions. This can be attributed to the fact that compressive loading was identified as the dominant loading direction at the distal radius [20].

In terms of the approach for quantifying remodelling events, we utilised a cluster filtering strategy to eliminate image artefacts. Filtering small structural clusters may remove genuine biological changes below the specified threshold, however the step is widely employed to supress known image artefacts arising from noise, beam hardening, and interpolation [17,18,55]. A consequence of the filtering method employed is that bone remodelling over a short follow-up interval is likely not detectable. This is evidenced by the detected remodelling fractions between the baseline and 1-month repeat scans (approximately 3%) falling within the same range that is observed in the error rate measured with same-day repeat scans. Therefore, our analysis is particularly relevant when a reasonable amount of remodelling is expected, for example, due to higher metabolic activity or a longer follow-up time.

Although our results show promising precision of our method for high-quality images, patient motion remains an issue for longitudinal

HR-pQCT investigations. As a result, we had to exclude many participants in the longitudinal cohort due to patient motion. This is consistent with other studies investigating bone mechanoregulation using HR-pQCT that included subsets of 9 out of 126 [19], 21 out of 102 [18] and 25 out of 106 participants [21]. Future advances in motion suppression, whether through computational or hardware approaches, will be necessary to move HR-pQCT-based bone remodelling methods closer to clinical implementation. Further, HR-pQCT is limited to the peripheral skeletal sites. Therefore, direct assessment identification of reduced mechanoregulation at osteoporotic fracture sites with higher bone turnover rates, such as the hip or spine, is not yet possible. However, with the advent of new imaging technologies such as photon counting computed tomography [51] the application of mechanoregulation to other skeletal sites of interest could be possible in the future.

The combination of time-lapsed bone remodelling with micro-finite element analysis provides a powerful tool for investigating skeletal adaptation to mechanical load. This work provides the necessary filtering protocol to identify the true bone formation and resorption sites using longitudinal HR-pQCT. Further, we propose patient-specific bone mechanoregulation imaging markers and report their precision to aid in designing future clinical studies investigating bone mechanoregulation *in vivo*. Bone mechanoregulation markers have the potential to help decipher the underlying causes of abnormal bone remodelling in many

osteodegenerative disorders and age-related bone loss. Future research should determine whether these markers can be utilised to identify patients at risk for fracture and develop individualised mechanical treatment regimens.

CRediT authorship contribution statement

Matthias Walle: Conceptualization, Methodology, Software, Validation, Formal analysis, Investigation, Resources, Data curation, Writing – original draft, Writing – review & editing, Visualization. **Danielle E. Whittier:** Conceptualization, Methodology, Validation, Formal analysis, Investigation, Data curation, Writing – original draft, Writing – review & editing. **Denis Schenk:** Data curation, Writing – review & editing. **Penny R. Atkins:** Data curation, Writing – review & editing. **Michael Blauth:** Data curation, Writing – review & editing, Project administration. **Philippe Zysset:** Data curation, Writing – review & editing, Project administration. **Kurt Lippuner:** Data curation, Writing – review & editing, Project administration. **Ralph Müller:** Data curation, Writing – review & editing, Project administration, Funding acquisition, Supervision. **Caitlyn J. Collins:** Conceptualization, Methodology, Formal analysis, Data curation, Writing – review & editing, Project administration, Supervision.

Declaration of competing interest

The authors declare that they have no conflict of interest.

Data availability

The data and analytic code for this study may be made available from the corresponding author upon reasonable request.

Acknowledgements

Appendix A. Supplementary data

Supplementary data to this article can be found online at https://doi.org/10.1016/j.bone.2023.116780.

References

[1] A.A. Biewener, Safety factors in bone strength, Calcif. Tissue Int. 53 (1993) S68–S74, https://doi.org/10.1007/BF01673406.

[2] M.B. Schaffler, W.Y. Cheung, R. Majeska, O. Kennedy, Osteocytes: master orchestrators of bone, Calcif. Tissue Int. 94 (2014) 5–24, https://doi.org/10.1007/S00223-013-9790-Y/FIGURES/3.

[3] M.B. Schaffler, O.D. Kennedy, Osteocyte signaling in bone, Curr. Osteoporos. Rep. 10 (2012) 118–125, https://doi.org/10.1007/S11914-012-0105-4/FIGURES/1.

[4] L. Qin, W. Liu, H. Cao, G. Xiao, Molecular mechanosensors in osteocytes, Bone Res. 8 (2020) 1–24, https://doi.org/10.1038/s41413-020-0099-y.

[5] B. Martin, Mathematical model for repair of fatigue damage and stress fracture in osteonal bone, J. Orthop. Res. 13 (1995) 309–316, https://doi.org/10.1002/JOR.1100130303.

[6] E.J. Bassey, M.C. Rothwell, J.J. Littlewood, D.W. Pye, Pre- and postmenopausal women have different bone mineral density responses to the same high-impact exercise, J. Bone Miner. Res. 13 (1998) 1805–1813, https://doi.org/10.1359/JBMR.1998.13.12.1805.

[7] R. Chow, J.E. Harrison, C. Notarius, Effect of two randomised exercise programmes on bone mass of healthy postmenopausal women, Br. Med. J. (Clin. Res. Ed.) 295 (1987) 1441–1444, https://doi.org/10.1136/BMJ.295.6611.1441.

[8] G.F. Maddalozzo, C.M. Snow, High intensity resistance training: effects on bone in older men and women, Calcif. Tissue Int. 66 (2000) 399–404, https://doi.org/10.1007/S002230010081.

[9] G.F. Muschler, H. Nitto, C.A. Boehm, K.A. Easley, Age- and gender-related changes in the cellularity of human bone marrow and the prevalence of osteoblastic progenitors, J. Orthop. Res. 19 (2001) 117–125, https://doi.org/10.1016/S0736-0266(00)00010-3.

[10] G. D'Ippolito, P.C. Schiller, C. Ricordi, B.A. Roos, G.A. Howard, Age-related osteogenic potential of mesenchymal stromal stem cells from human vertebral bone marrow, J. Bone Miner. Res. 14 (1999) 1115–1122, https://doi.org/10.1359/JBMR.1999.14.7.1115.

[11] Y. Koshihara, A. Suematsu, D. Feng, R. Okawara, H. Ishibashi, S. Yamamoto, Osteoclastogenic potential of bone marrow cells increases with age in elderly women with fracture, Mech. Ageing Dev. 123 (2002) 1321–1331, https://doi.org/10.1016/S0047-6374(02)00071-4.

[12] E.A. Tonna, Electron microscopic study of bone surface changes during aging.The loss of cellular control and biofeedback, J. Gerontol. 33 (1978) 163–177, https://doi.org/10.1093/GERONJ/33.2.163.

[13] S. Qiu, D.S. Rao, S. Palnitkar, A.M. Parfitt, Relationships between osteocyte density and bone formation rate in human cancellous bone, Bone 31 (2002) 709–711, https://doi.org/10.1016/S8756-3282(02)00907-9.

[14] Z. Seref-Ferlengez, S.O. Suadicani, M.M. Thi, A new perspective on mechanisms governing skeletal complications in type 1 diabetes, Ann. N. Y. Acad. Sci. 1383 (2016) 67, https://doi.org/10.1111/NYAS.13202.

[15] S.L. Manske, Y. Zhu, C. Sandino, S.K. Boyd, Human trabecular bone microarchitecture can be assessed independently of density with second generation HR-pQCT, Bone 79 (2015) 213–221, https://doi.org/10.1016/j.bone.2015.06.006.

[16] S. Boutroy, M.L. Bouxsein, F. Munoz, P.D. Delmas, In vivo assessment of trabecular bone microarchitecture by high-resolution peripheral quantitative computed tomography, J. Clin. Endocrinol. Metab. 90 (2005) 6508–6515, https://doi.org/10.1210/JC.2005-1258.

[17] P. Christen, S. Boutroy, R. Ellouz, R. Chapurlat, B. van Rietbergen, Least-detectable and age-related local in vivo bone remodelling assessed by time-lapse HR-pQCT, 2018, https://doi.org/10.1371/journal.pone.0191369.

[18] M.E. Mancuso, K.L. Troy, Relating bone strain to local changes in radius microstructure following 12 months of axial forearm loading in women, J. Biomech. Eng. 142 (2020) 1–11, https://doi.org/10.1115/1.4048232.

[19] P. Christen, K. Ito, R. Ellouz, S. Boutroy, E. Sornay-Rendu, R.D. Chapurlat, B. van Rietbergen, Bone remodelling in humans is load-driven but not lazy, Nat. Commun. 5 (2014) 1–5, https://doi.org/10.1038/ncomms5855.

[20] M. Walle, F.C. Marques, N. Ohs, M. Blauth, R. Müller, C.J. Collins, Bone mechanoregulation allows subject-specific load estimation based on time-lapsed micro-CT and HR-pQCT in vivo, Front. Bioeng. Biotechnol. 9 (2021) 486, https://doi.org/10.3389/fbioe.2021.677985.

[21] C.J. Collins, P.R. Atkins, N. Ohs, M. Blauth, K. Lippuner, R. Müller, Clinical observation of diminished bone quality and quantity through longitudinal HR-pQCT-derived remodeling and mechanoregulation, Sci. Rep. 12 (2022) 1–13, https://doi.org/10.1038/s41598-022-22678-z.

[22] M.G. Goff, C.R. Slyfield, S.R. Kummari, E.v. Tkachenko, S.E. Fischer, Y.H. Yi, M.G. Jekir, T.M. Keaveny, C.J. Hernandez, Three-dimensional characterization of resorption cavity size and location in human vertebral trabecular bone, Bone 51 (2012) 28, https://doi.org/10.1016/J.BONE.2012.03.028.

[23] E.F. Eriksen, H.J.G. Gundersen, F. Melsen, L. Mosekilde, E.F. Eriksen, Reconstruction of the formative site in iliac trabecular bone in 20 normal individuals employing a kinetic model for matrix and mineral apposition, 1984.

[24] F.A. Schulte, D. Ruffoni, F.M. Lambers, D. Christen, D.J. Webster, G. Kuhn, R. Müller, Local mechanical stimuli regulate bone formation and resorption in mice at the tissue level, PLoS One 8 (2013), e62172, https://doi.org/10.1371/JOURNAL.PONE.0062172.

[25] H.E. Plesser, Reproducibility vs. replicability: a brief history of a confused terminology, Front. Neuroinform. 11 (2018) 76, https://doi.org/10.3389/FNINF.2017.00076/BIBTEX.

[26] M. Walle, D. Eggemann, P.R. Atkins, J.J. Kendall, K. Stock, R. Müller, C.J. Collins, Motion grading of high-resolution quantitative computed tomography supported by deep convolutional neural networks, Bone 166 (2023), 116607, https://doi.org/10.1016/J.BONE.2022.116607.

[27] D. Schenk, A. Mathis, K. Lippuner, P. Zysset, In vivo repeatability of homogenized finite element analysis based on multiple HR-pQCT sections for assessment of distal radius and tibia strength, Bone 141 (2020), 115575, https://doi.org/10.1016/J.BONE.2020.115575.

[28] S. Bonaretti, S. Majumdar, T.F. Lang, S. Khosla, A.J. Burghardt, The comparability of HR-pQCT bone measurements is improved by scanning anatomically standardized regions, Osteoporos. Int. 28 (2017) 2115–2128, https://doi.org/10.1007/S00198-017-4010-7/TABLES/7.

[29] P.R. Atkins K. Stock N. Ohs C.J. Collins L. Horling S. Benedikt G. Degenhart K. Lippuner M. Blauth P. Christen , others, Formation Dominates Resorption with Increasing Mineralized Density and Time-Post-Fracture in Cortical but not Trabecular Bone: A Longitudinal HR-pQCT Imaging Study in the Distal Radius, JBMR Plus. (n.d.) e10493.

[30] P.R. Atkins K. Stock N. Ohs C.J. Collins L. Horling S. Benedikt G. Degenhart K. Lippuner M. Blauth P. Christen , others, Formation Dominates Resorption with Increasing Mineralized Density and Time-Post-Fracture in Cortical but not Trabecular Bone: A Longitudinal HR-pQCT Imaging Study in the Distal Radius, JBMR Plus. (n.d.) e10493.

[31] D.E. Whittier, S.K. Boyd, A.J. Burghardt, J. Paccou, A. Ghasem-Zadeh, R. Chapurlat, K. Engelke, M.L. Bouxsein, Guidelines for the assessment of bone density and microarchitecture in vivo using high-resolution peripheral quantitative computed tomography, Osteoporos. Int. 31 (2020) 1607–1627, https://doi.org/10.1007/s00198-020-05438-5.

[32] H.R. Buie, G.M. Campbell, R.J. Klinck, J.A. MacNeil, S.K. Boyd, Automatic segmentation of cortical and trabecular compartments based on a dual threshold technique for in vivo micro-CT bone analysis, Bone 41 (2007) 505–515, https://doi.org/10.1016/j.bone.2007.07.007.

[33] D.E. Whittier, A.N. Mudryk, I.D. Vandergaag, L.A. Burt, S.K. Boyd, Optimizing HR-pQCT workflow: a comparison of bias and precision error for quantitative bone analysis, Osteoporos. Int. 31 (2020) 567–576, https://doi.org/10.1007/S00198-019-05214-0/TABLES/3.

[34] Z. Yaniv, B.C. Lowekamp, H.J. Johnson, R. Beare, SimpleITK image-analysis notebooks: a collaborative environment for education and reproducible research, J. Digit. Imaging 31 (2018) 290–303, https://doi.org/10.1007/S10278-017-0037-8.

[35] R. Beare, B. Lowekamp, Z. Yaniv, Image segmentation, registration and characterization in R with SimpleITK, J. Stat. Softw. 86 (2018), https://doi.org/10.18637/JSS.V086.I08.

[36] C.-C. Gliier, G. Blake, Y. Lu, B.A. Blunt, M. Jergas, H.K. Genant, in: Osteoporosis international accurate assessment of precision errors: how to measure the reproducibility of bone densitometrytechniques 5, 1995, pp. 262–270.

[37] D.E. Whittier, S.L. Manske, D.P. Kiel, M. Bouxsein, S.K. Boyd, Harmonizing finite element modelling for non-invasive strength estimation by HR-pQCT, J. Biomech. 80 (2018) 63, https://doi.org/10.1016/J.JBIOMECH.2018.08.030.

[38] C. Flaig, P. Arbenz, A scalable memory efficient multigrid solver for micro-finite element analyses based on CT images, Parallel Comput. 37 (2011) 846–854, https://doi.org/10.1016/j.parco.2011.08.001.

[39] D.C.T. né Betts, E. Wehrle, G.R. Paul, G.A. Kuhn, P. Christen, S. Hofmann, R. Müller, D.C. Tourolle né Betts, E. Wehrle, G.R. Paul, G.A. Kuhn, P. Christen, S. Hofmann, R. Müller, The association between mineralised tissue formation and the mechanical local in vivo environment: time-lapsed quantification of a mouse defect healing model, Sci. Rep. 10 (2020) 1–10, https://doi.org/10.1038/s41598-020-57461-5.

[40] L. Wang, X. You, L. Zhang, C. Zhang, W. Zou, Mechanical regulation of bone remodeling, Bone Res. 10 (2022) 1–15, https://doi.org/10.1038/s41413-022-00190-4.

[41] S.L. Manske, E.M. Davison, L.A. Burt, D.A. Raymond, S.K. Boyd, The estimation of second-generation HR-pQCT from first-generation HR-pQCT using in vivo cross-calibration, J. Bone Miner. Res. 32 (2017) 1514–1524, https://doi.org/10.1002/jbmr.3128.

[42] S.C. Manolagas, A.M. Parfitt, What old means to bone, Trends Endocrinol. Metab. 21 (2010) 369–374, https://doi.org/10.1016/j.tem.2010.01.010.

[43] A.M. Parfitt, Misconceptions (2): turnover is always higher in cancellous than in cortical bone, 2002.

[44] A.M. Parfitt, D.S. Rao, J. Stanciu, A.R. Villanueva, M. Kleerekoper, B. Frame, Irreversible bone loss in osteomalacia. Comparison of radial photon absorptiometry with iliac bone histomorphometry during treatment, J. Clin. Investig. 76 (1985) 2403–2412, https://doi.org/10.1172/JCI112253.

[45] S. Salam, O. Gallagher, F. Gossiel, M. Paggiosi, A. Khwaja, R. Eastell, Diagnostic accuracy of biomarkers and imaging for bone turnover in renal osteodystrophy, J. Am. Soc. Nephrol. 29 (2018) 1557–1565, https://doi.org/10.1681/ASN.2017050584/-/DCSUPPLEMENTAL.

[46] M. Walle, D.E. Whittier, M. Frost, R. Müller, C.J. Collins, Meta-analysis of diabetes mellitus-associated differences in bone structure assessed by high-resolution peripheral quantitative computed tomography, Curr. Osteoporos. Rep. (2022), https://doi.org/10.1007/s11914-022-00755-6.

[47] A. Parajuli, C. Liu, W. Li, X. Gu, X. Lai, S. Pei, C. Price, L. You, X.L. Lu, L. Wang, Bone's responses to mechanical loading are impaired in type I diabetes, Bone 81 (2015) 152, https://doi.org/10.1016/J.BONE.2015.07.012.

[48] K.L. Troy, M.E. Mancuso, J.E. Johnson, Z. Wu, T.J. Schnitzer, T.A. Butler, Bone adaptation in adult women is related to loading dose: a 12-month randomized controlled trial, J. Bone Miner. Res. 35 (2020) 1300–1312, https://doi.org/10.1002/JBMR.3999.

[50] T. Sugiyama, Physical activity and bone health: understanding mechanical strain-related stimuli, Int. J. Epidemiol. 47 (2018) 669–670, https://doi.org/10.1093/IJE/DYY037.

[51] M. Bonvento, T. Button, P. Srivastava, E. Roessl, R. Proksa, K-edge imaging in X-ray computed tomography using multi-bin photon counting detectors, Phys. Med. Biol. 52 (2007) 4679, https://doi.org/10.1088/0031-9155/52/15/020.

[52] H. Razi, A.I. Birkhold, R. Weinkamer, G.N. Duda, B.M. Willie, S. Checa, Aging leads to a dysregulation in mechanically driven bone formation and resorption, J. Bone Miner. Res. 30 (2015) 1864–1873, https://doi.org/10.1002/JBMR.2528.

[53] M.R. Allen, D.B. Burr, Techniques in histomorphometry, Basic Appl. Bone Biol. (2014) 131–148, https://doi.org/10.1016/B978-0-12-416015-6.00007-1.

[54] R.K. Surowiec, E.A. Swallow, S.J. Warden, M.R. Allen, Tracking changes of individual cortical pores over 1 year via HR-pQCT in a small cohort of 60-year-old females, Bone Rep. 17 (2022), 101633, https://doi.org/10.1016/j.bonr.2022.101633.

[55] D.E. Whittier, L.A. Burt, S.K. Boyd, A new approach for quantifying localized bone loss by measuring void spaces, Bone 143 (2021), https://doi.org/10.1016/J.BONE.2020.115785.

[56] A. Malhotra, M. Walle, G.R. Paul, G.A. Kuhn, R. Müller, Application of subject-specific adaptive mechanical loading for bone healing in a mouse tail vertebral defect, Sci. Rep. 11 (2021) 1–10, https://doi.org/10.1038/s41598-021-81132-8.

[57] G.R. Paul, P. Vallaster, M. Rüegg, A.C. Scheuren, D.C. Tourolle, G.A. Kuhn, E. Wehrle, R. Müller, Tissue-level regeneration and remodeling dynamics are driven by mechanical stimuli in the microenvironment in a post-bridging loaded femur defect healing model in mice, Front Cell Dev. Biol. 10 (2022) 906, https://doi.org/10.3389/FCELL.2022.856204/BIBTEX.

[58] F.C. Marques, D. Boaretti, M. Walle, A.C. Scheuren, F.A. Schulte, R. Müller, Mechanostat parameters estimated from time-lapsed in vivo micro- computed tomography data of mechanically driven bone adaptation are logarithmically dependent on loading frequency, Front. Bioeng. Biotechnol. Sect. Biomech. 11 (2023).